Journal of Engineering Research

Volume 6 | Issue 5 Article 20

2022

Optimized Adaptive Frangi-based Coronary Artery Segmentation using Genetic Algorithm

Ahmed Hawas, Mohamed Elsayed Elsetiha, Heba El-Khobby, Amira Ashour

Vol. 6, No. 5 – 2022 Journal of Engineering Research (ERJ)

Optimized Adaptive Frangi-based Coronary Artery Segmentation using Genetic Algorithm

Ahmed R. Hawas[a,*], Mohamed Elsayed Elsetiha[b], Heba Ali El-Khobby[a], Amira S. Ashour[a]

[a]Electronics and Electrical Communication Engineering Department, Faculty of Engineering, Tanta University, 31527, Egypt
[b]Department of Heart and Blood Vessel, Faculty of Medicine, Tanta University, 31527, Egypt
*Corresponding Author E-Mail Address: ahmed.hawas@f-eng.tanta.edu.eg

Abstract- **Coronary arteries' diseases are deliberated as one of the most common heart diseases leading to death worldwide. For their early detection, the X-ray angiography is uses as a benchmark imaging modality for diagnosis. The acquired X-ray angiography images usually suffer from low quality, and the presence of noise. Therefore, for developing a computer-aided diagnosis (CAD) system, vessel enhancement and segmentation play significant role. In this paper, an optimized adapted filter based on Frangi filter was proposed for superior segmentation of the angiography images using genetic algorithm (GA). The original angiography images were initially preprocessed to enhance their contrast followed by generating the vesselness map using the proposed optimized Frangi filter. Then, a segmentation technique was applied to extract only the main artery vessel. The experimental results on angiography images established the superiority of the vessel regions extraction showing 98.58% accuracy compared to the state-of-the-art.**

Keywords- **Angiography; vessel segmentation; Frangi filter; genetic algorithm; stenosis.**

1. INTRODUCTION

X-ray coronary angiogram is a gold standard in cardiology for evaluating/monitoring irregularities of the coronary artery. The main three coronary artery branches are left circumflex artery (LCX), the right coronary artery (RCA), and left anterior descending artery (LAD). Automated segmentation of coronary artery has a significant role in the development of CAD systems to support the recognition of coronary heart diseases. For medical image segmentation, a preprocessing phase is essential to improve the further stages and identify the tubular structures for efficient clinical practice on cardiovascular diseases. Several methods based on Frangi filter [1] and Hessian matrix have been applied for the enhancement for further segmentation and detection of the vessels in different medical applications [2, 3]. Likewise, Cui *et al.* [4] implemented a modified Frangi filter that multiplies an exponential term by the original Frangi filter to tackle the non-smoothness problem in the origin image and improve the identification of the targeted tubular structures from the nearby tissues. For coronary artery segmentation, Matthias *et al.* [5] designed an automated robust histogram-based threshold method to generate the vessel tree. In retinal images, Cervantes *et al.* [6] implemented a vessel segmentation scheme by fine tuning the different parameters using the genetic algorithms to achieve high quality of vessel segmentation. In coronary arteries in X-ray angiograms, Cruz-Aceves *et al.* [7] developed an automated segmentation using multiscale Gabor filter for vessel structures' detection. In addition, Tenekeci *et al.* [8] determined the position of the vessel structure in the XCA image. The deteriorated performance of the different segmentation methods of the coronary artery's vessels was due to different limitations including the calcified arteries, arteries narrowed/discontinues branches, leading to imprecise extraction of the vessels. However, the most popularly used vesselness measure includes Frangi filter, which approximates the vessel by a tubular structure [9].

From the preceding studies, Frangi filter is considered one of the most common filters with angiography images. This paper aims to enhance the performance of Frangi filter by proposing a vessel extraction model for detecting the RCA using optimized adaptive Frangi filter. To extract coronary arteries, the location of the stenosis starts from seed points in the region growing segmentation as offered in this paper. In this approach, the proposed vessel extraction model is divided into two stages, namely 1) determining the optimal parameters of the adaptive Frangi filter, and 2) applying the optimal parameters for vessel extraction. Accordingly, a new process was proposed to determine the lower and upper boundary for different parameters for speeding-up the searching process to obtain the optimal values.

2. METHODOLOGY

In this section, the details of the proposed system are demonstrated in Fig. 1 showing the complete flow of the proposed system, including two main modules, namely pre-processing, and segmentation, respectively. In this paper, an optimized adaptive Frangi filter was proposed to detect the RCA vessel by finding the optimal values across the whole processes. The details of each module in the proposed method are defined in the following subsections, including contrast adjustment, and vesselness map.

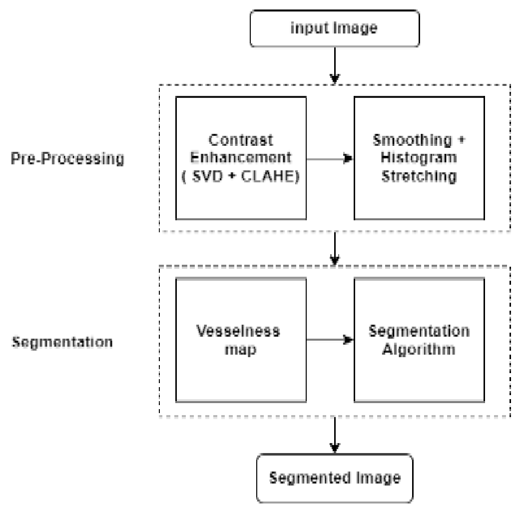

Figure 1. Block diagram of the proposed method of the main vessel extraction.

A. Preprocessing

One of the most challenging limitations affecting the angiography images is their low contrast causing an obstacle to distinguish between the vessels and the background. So, the main objective of the preprocessing stage is to facilitate the segmentation process through enhancing the input image's contrast without adding extra noise. The original image is passed through three main steps, namely: a) contrast adjustment, b) contrast equalization, and c) smoothing and histogram stretching as illustrated in Fig.1. Since the Singular Value Decomposition (SVD) [10] is one of the contrast adjustment techniques, which is used in the proposed system. It controls the determination of the chosen contrast level for enhancing the contrast based on the image itself. Improving the images' contrast is significant, where the illumination has a great effect. In this paper, the SVD was applied, where a matrix signifying the SVD of any image can be formulated as follows [10]:

$$I_{(U,S,A)} = U * S * A \quad (1)$$

where *U*, and *A* are square matrices, called hanger and aligner, respectively, also, *S* is a matrix of the singular terms along the diagonal that represents the image's intensity information. Changing these singular terms modifies the image's intensity profile that improves the equalization process. The resultant matrix of the SVD yields to the preferred singular terms as follows [11]:

$$F = \frac{\max(S_{N\,(\mu=128,\mathrm{var}=0)})}{\max(S)} \quad (2)$$

where $S_{N(\mu=128,var=0)}$ signifies the matrix of artificial intensity singular values. After applying the equalization steps, the equalized image is regenerated and expressed as follows:

$$I_{(U,S,A)} = U * S * F.A \quad (3)$$

Then, the histogram equalization is performed using contrast-limited adaptive histogram equalization (CLAHE) method [12] to enhance the images having low contrast. It reduces the noise by handling small regions, called tiles, instead of the entire image. The histogram of the enhanced region is almost matches a specific histogram, so the adjacent tiles are then joint using bilinear interpolation for eliminating the boundaries. In homogeneous regions, the contrast can be restricted for avoiding noise amplification. The output image of the histogram equalizer is then processed using smoothing filter (guided filter) [13] to filter out the noise while keeping the boundaries of the sharp objects. The lower value at the generated guided image is limited by 90% of the 1st percentiles of the guided image. Finally, the image is stretched using the following formula [14]:

$$\begin{gathered} thr = prctile(Im, 1) * 0.9 \\ Im(Im \leq thr) = thr \\ Im` = \frac{Im - thr}{\max(Im)} \end{gathered} \quad (4)$$

B. Segmentation based on Vesselness map

The segmentation of the coronary artery is based on multiscale image analysis, which adds a new space to the original image. New versions of the image are produced based on a scale value and the original image [15] by convolving the original image $\mathrm{Im}_{org}(x,y)$ with the Gaussian filter $G_\sigma(x,y)$ for representing the image at a definite scale σ as follows:

$$\mathrm{Im}_\sigma(x,y) = \mathrm{Im}_{org}(x,y) \otimes G_\sigma(x,y) \quad (5)$$

where (*x*,*y*) is the pixel location, $\otimes$ is the convolution operator, and $G_\sigma(x,y)$, which is given by:

$$G_\sigma(x,y) = \frac{1}{\sqrt{2\pi\sigma}} \exp - \frac{(x^2+y^2)}{2\sigma^2} \quad (6)$$

where $\sigma \in \sum\{\sigma_{\min},....,\sigma_{\max}\}$, $\sigma_{\min}$ and $\sigma_{\max}$ are sets consistent with the approximate width of the smallest, and largest detected vessel, respectively.

The main advantage of this new scale space is that second order derivative can be calculated directly from the convolution with derivatives of Gaussian. Thus, the Hessian matrix can be calculated at each point by [16]:

$$Hu_\sigma(x,y) = \left[\begin{pmatrix} \frac{\partial^2 \mathrm{Im}_\sigma(x,y)}{\partial x^2} & \frac{\partial^2 \mathrm{Im}_\sigma(x,y)}{\partial x\,\partial y} \\ \frac{\partial^2 \mathrm{Im}_\sigma(x,y)}{\partial x\,\partial y} & \frac{\partial^2 \mathrm{Im}_\sigma(x,y)}{\partial y^2} \end{pmatrix}\right] \quad (7)$$

The Hessian matrix has two real eigenvalues λ_1 and λ_2 and two related eigenvectors e_1 and e_2. The relative and absolute magnitudes along with the signs of the eigenvalues describe the intensity's local shape in the image. For angiography images, a pixel belonging to a vessel region is signified by black color, and its eigenvalues are closed to zero ($\lambda_1 = 0$) with high λ_2 positive value, where ($\lambda_1 < \lambda_2$).
Frangi geometrically interprets the principal vessel curvatures from Hessian eigenvalues with providing vesselness measure. Two components are produced that describe object structures in the images:

i) $R = \lambda_1 / \lambda_2$ which is the blob-like structure measure, and
ii) $S_p = \sqrt{\lambda_1^2 + \lambda_2^2}$ which is second-order structure-ness measure, called the Frobenius norm of the Hessian matrix.

These components were combined in a function to describe the vesselness as [1]:

$$V(x,y) = \begin{cases} 0 & if\ \lambda_2 < 0 \\ \exp(-\frac{R^2}{2\eta^2})(1-\exp(-\frac{S_b{}^2}{2\kappa^2})) & if\ \lambda_2 \geq 0 \end{cases} \quad (8)$$

where η and K are tuned parameters that control the sensitivity of the filter to R and S_b , respectively. Also, $V(x,y)$ becomes maximum only when the vessel's width in pixel (x,y) counterparts an appropriate scale factor σ according to the multiscale concept. Therefore, for multi-scale vessel enhancement, *V* is calculated at different scales, afterward, the maximum value is considered. The filter's final output can be given by:

$$V_{\max}(x,y) = \max_{\sigma\in\Sigma}(V_\sigma(x,y)) \quad (9)$$

Vol. 6, No. 5 – 2022 Journal of Engineering Research (ERJ)

For segmentation, Hessian matrix provides information related to the direction of optical flow through the objects, i.e. the vessels where e_1 provides the direction of the potential linear structure, whereas e_2 gives its normal direction. Consequently, the vessel direction information D_σ can be represented as:

$$D_\sigma(x,y)=\begin{cases}0 & if\ \lambda_2<0\\ e1 & o.w\end{cases} \quad (10)$$

At the location of the coronary artery stenosis, the filter response considerably decreases. Nevertheless, the direction matrix ensures the continuousness of the concerned pixels and their neighbors. To find proper vesselness map, Frangi is applied as it has high immunity to noise. Also, it is more robust for vessel detection. Hence, the output of the previous stage is passed through Frangi filter to obtain the vesselness map, which will be used on the segmentation process. Beginning from the highest scale of $\sigma_{\max}$ till $\sigma_{\min}$, the vesselness (V) and direction (D_σ) features are calculated for each scale, and the maximum values are chosen across the multiscale version to construct the output image. Based on these multiscale geometrical and direction information, a robust multiscale region growing segmentation is introduced and applied by Kerkeni *et al*. [17] to track thin and wide vessels. For all pixels (x,y) having any neighbors equal to 1, and $V_\sigma(x,y)>\alpha*(1-\omega_\sigma((x,y),(x_n,y_n)))$, where α is a tunable parameter of the vesselness value required to grow the vessel area. For normalized vesselness value between [0, 1], the smaller vesselness value can cause over-growth of the vessel constituency, although the biggest one limits the extension of these points. Then, $I_{seg}(x,y)=1$, where ω_σ is the correlation between the two pixels originations, which is given by:

$$\omega_\sigma((x,y),(x_n,y_n))=\frac{D_\sigma(x,y).D_\sigma(x_n,y_n)}{\|D_\sigma(x,y)\|\|D_\sigma(x_n,y_n)\|} \quad (11)$$

where $\omega_\sigma((x,y),(x_n,y_n))$ has value close to one when these two local directions are parallel. The vessel segmentation result is incredibly increased due to use a combination between the vesselness response, and the vessel direction information. Thus, neighbors showing directions close to the seed point direction even if their vesselness responses are less than an assumed threshold (α). This assists the segmentation continuity lengthwise the artery direction as well as diminishes the number of broken branches. Then, a region growing procedure is performed to determine the initial seed points of the regional growing process, where top pixels with the highest Frangi vesselness response are selected. Some top pixels are being ignored based on the predefine spacing Euclidean distance (Ed) threshold as these points are already neighbor of selected seed points that will increase our system performance. Finally, the component analysis is executed to extract the largest object representing the RoI.

From the previous analysis, there are several tunable parameters that have direct effect on the vessel segmentation results. To determine the weight and effect for each parameter a try and error mechanism was carried out to select the main parameters to be tuned using the GA optimization technique. Hence, the proposed system aims to get the optimal values for the tunable parameters, which increase the credibility of the proposed segmentation system to deal with different types, and shapes of arteries. Six parameters were selected for further tuning, namely the three sigma parameters $\sigma_{\min},\sigma_{\max},\sigma_{step}$ are selected as they control the vesselness response based on artery size, along with tuning the regional growing process by adjusting the best value for α as well as the number of seeds points (Ns), and the log distance. Such parameters are selected for further tuning, as a small number of points leads to deteriorated segmentation results, and a large number of initial seed points leads to over segmentation.

Therefore, the proposed method provided a reliable way to search for the most suitable values using the GA. Initially, the exact boundary ranges for each of these tunable parameters were determined to speed the optimization process. Typically, unsuitable setting of $\sigma_{\min},\sigma_{\max}$ leads to failure of the segmentation process, where very small $\sigma_{\min}$ leads to detecting very tiny vessels which are out of interest. Also, large value for $\sigma_{\max}$ increases the boarder thickness of the vessel, which reduces the overall segmentation accuracy. Thus, $\sigma_{\min},\sigma_{\max}$ were chosen according to the largest, and smallest vessel thickness. The lower and upper boundary limits were set according to the average of the minimum and maximum diameters for all ground-truth images. Consequently, we perform an extra step to know the range of the vessel thickness size in our dataset. The diameter of vessel was calculated based on sequence of morphological operations on the binary image as illustrated in Fig. 2.

To compute the vessel radius, the central line of the vessel is determined, then the Euclidian distance is calculated between each point on it to the border line. Consequently, the Euclidean distance transform (EDT) of the inverse binary image was computed. The distance for all points related to the vessel are obtained to skeletonize the binary image for further use to mask the EDT image for obtaining an image with values only along the centerline of the vessel. This gives all the radii along the axis of the vessel. Finally, the minimum, and maximum radii are obtained, from which the diameters of the vessel are determined to be 2, and 26, respectively.

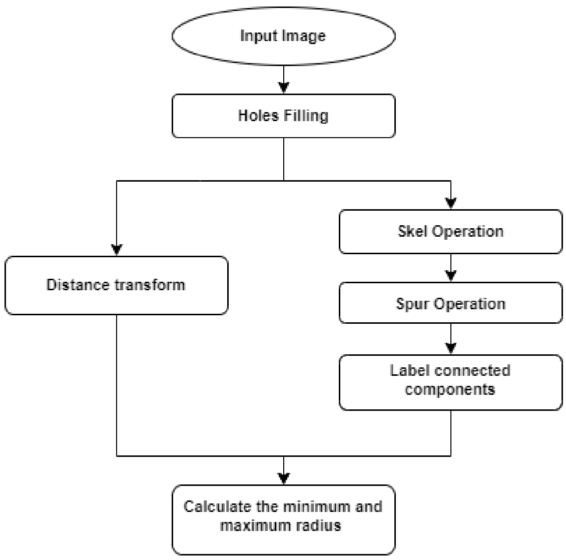

Figure 2. Flow diagram to calculate the minimum and maximum vessel radius.

C. Genetic Algorithm Optimizer

Once the boundaries of $\sigma_{\min}, \sigma_{\max}$ were determined, σ_{step} range can also be set to the same range for the lower and upper boundaries with constrain that these values cannot exceed $\sigma_{\max}$. In addition, the limiting value for α is [0:1], the number of seeds point is ranging [1:1000], and the log distance between each seed points is [0:10]. Figure 3 includes the flow diagram of the genetic algorithm procedure. The GA is accomplished using 5-fold cross-validation procedure to obtain the optimized values, and avoid any misleading values. Finally, the obtained optimal parameters' values are correlated using simple mathematical function, such as the average, the median, or the best function for selecting the best set of values to be considered as the optimal values for the whole training set.

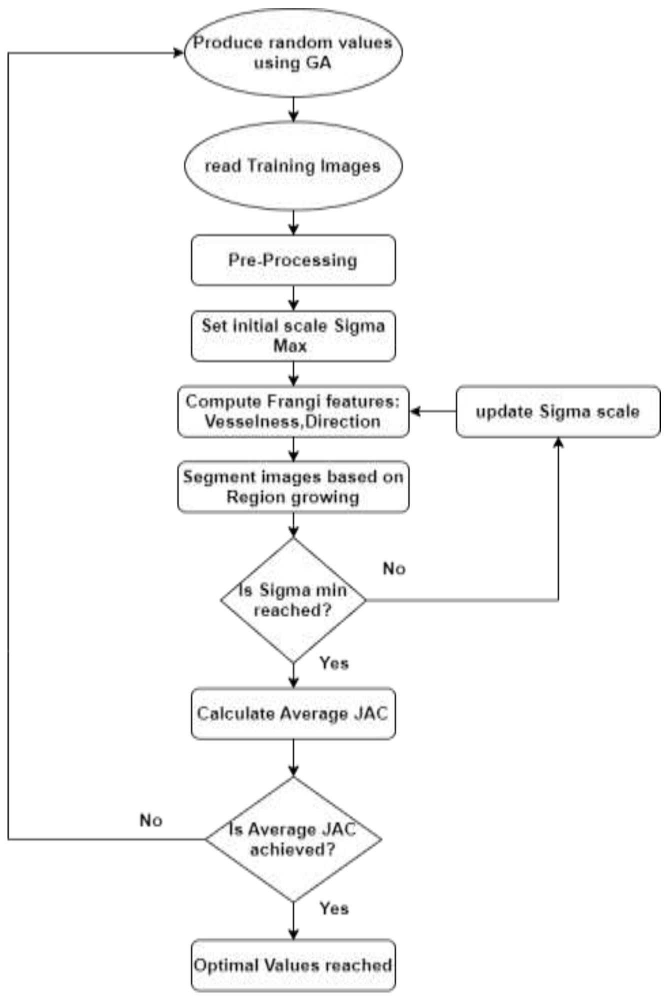

Figure 3. GA optimization flow diagram.

D. Performance evaluation metrics

Numerous performance metrics can be computed for evaluating the proposed vesselness segmentation system, including the Jaccard index (JAC), Dice coefficient, sensitivity, specificity, and accuracy, which are defined as follows. The JAC compares the diversity between the samples using the following formula [18]:

$$JAC(O,T) = \frac{A_O \cap A_T}{A_O \cup A_T} \quad (12)$$

where ∩ and ∪ are the intersection, and union of two sets, respectively, furthermore, A_o and A_T are the segmented and the reference images surrounded by the boundaries O and T; respectively. Furthermore, the Dice index likens the similarity of two sets O and T [19] as follows:

$$DIC(O,T) = \frac{2\,|A_O \cap A_T|}{|A_O| + |A_T|} \quad (13)$$

Additionally, the sensitivity, specificity, and accuracy are correlated to the recognition of the main branch, which are expressed as follows:

$$Sensitivity = \frac{|TP|}{|TP| + |FN|} \quad (14)$$

where TP is true positives, and FN is false negatives. The specificity is expressed as follows:

$$Specificity = \frac{|TN|}{|TN| + |FP|} \quad (15)$$

where TN is true negatives, and FP is false positives. The accuracy measures the dependability degree of a diagnostic test, which is given by [20]:

$$Accuracy = \frac{|TP| + |TN|}{|TP| + |TN| + |FP| + |FN|} \quad (16)$$

3. RESULTS AND DISCUSSION

A. Dataset Acquisition

Clinical X-ray angiograms were attained during cardiac catheter checkups using PHILIPS INTEGRIS H50000 F system available at OM EL-Kore Cardiac Center, Tanta, ElGharbia, Egypt. The used dataset consists of X-ray angiogram images of RCA view for 200 patients, where each patient has about 30 significant images. Each image in the used dataset has a size of 512x512 in gray scale format. The ground-truth images are manually labeled by an expert physician. Figure 4 illustrates sample images from the used dataset and their equivalent ground-truth images.

B. Software Specifications

An Intel CORE i7 processor running at 2.50GHz that has 16.0 GB RAM with Windows version 10 was used to conduct the experiments. MATLAB 2016b software was used to implement and evaluate the proposed model.

C. Proposed system evaluation results

During the experimental results for evaluating the proposed system, we used $\eta = 0.5$, and half the maximum Hessian norm for $K = 0.5\,\|\max(H(x))\|$. The GA is configured as shown in Table 1. In Table 1, the population's initial range of the tuned parameters of $\sigma_{\max}$ represents the maximum artery's radius found on the used dataset, while the range of $\sigma_{\min}$ was selected with a constrain that $\sigma_{\max}$ cannot be less than $\sigma_{\min}$. The convergence/iterative processes of the GA are shown in Fig. 5 illustrating the best/mean fitness values on the X-ray angiography training images.

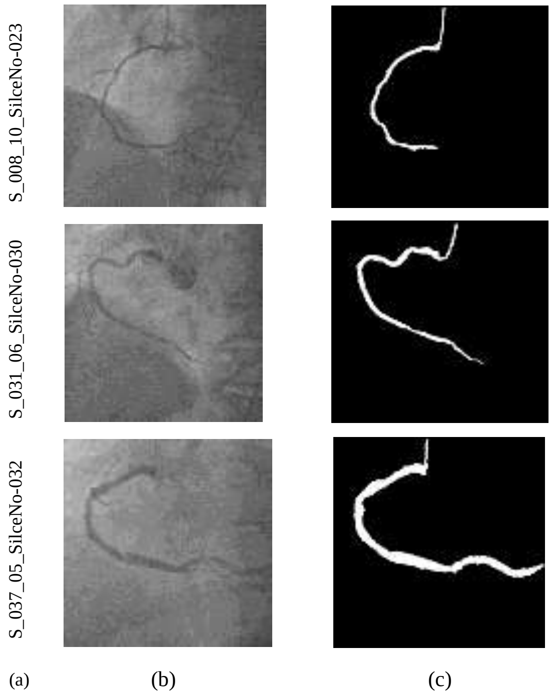

Figure 4. Sample of the used dataset including X-ray angiogram images in the RCA view, where (a) image ID, (b) original image, and (c) the corresponding ground-truth of each image.

Table 1. Genetic algorithm configuration.

Parameters/Function	**Settings/Range**
σ_{max}	[1 - 13]
σ_{min}	[1 - 2]
σ_{step}	[2 - 5]
α	[0 - 1]
N	[1 – 500]
Log distance (d)	[0 - 10]
Population Size	10
Unlimited Stall Generation Limit	$1e^{-4}$
Tolerance value of Fitness Limit	$1e^{-6}$
Number of generations	50
Fitness function	1-average(JAC)

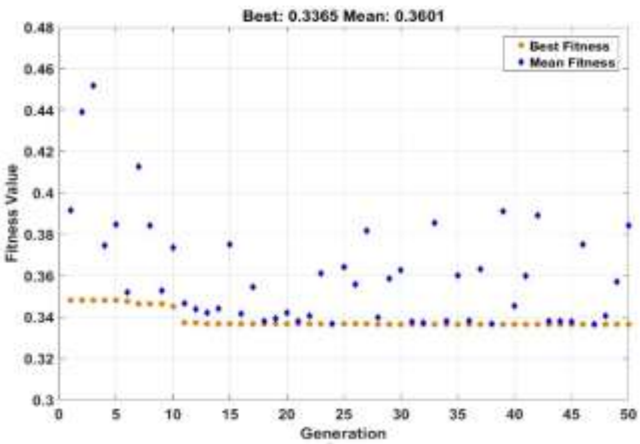

Figure 5. The best function value vs. the generation.

Table 2 the optimal values calculated after performing the iterations of the GA.

Function	σ_{max}	σ_{min}	σ_{step}	α	N	d
Average	8.043	1.549	6.875	0.948	118.125	4.75
Median	9.033	1.803	9.500	0.974	73	3
Best	9.530	1.805	6.000	0.999	186	3

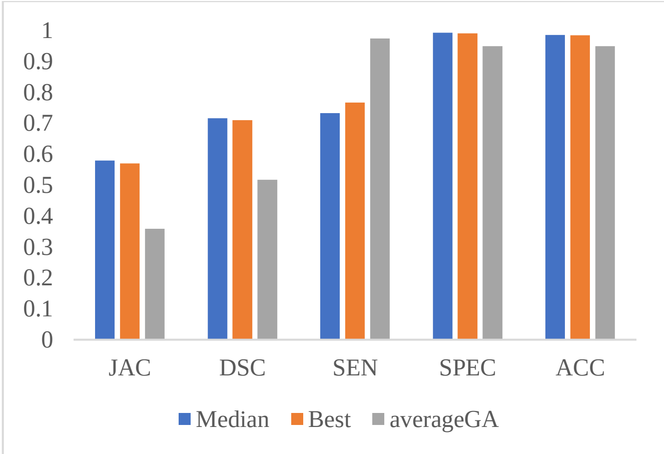

Figure 6. Comparison between the calculated optimal values in terms of the evaluation metrics.

In Fig. 5, the mean fitness indicates the average value of all fitness function's output over one generation, and the best fitness is the best population in this generation, where we run the GA on the training images set to find the optimal values for all images dataset. After performing all GA iterations for training and validation tasks. The average, median, and best values are being calculated across all the obtained results. After applying the corresponding mathematical function, the calculated values are used to examine the performance across the whole dataset. The best values are considering the optimal value set for the whole dataset.

From Table 2, the calculated values for σ_{min} are very close to each other, which are equivalent to the radius of the smallest detected vessel. Conversely, the other parameters have significant changes, which means each image can have its own optimal values, which inspired the proposed system to find the best values that fit the most number of images. A comparative study in terms of the evaluation metrics was conducted to show the effect of using the calculated parameters based on mathematical function for the whole dataset as shown on Fig. 6.

Regarding the JAC, the median values of the parameters have the highest dice and JAC values, median and best parameters have slightly equal evaluation values. The average parameters have higher sensitivity than using the best, and median parameters, but it has disadvantages of producing various false positives as proved by the low specificity, and accuracy values. Accordingly, Fig. 6 proved the efficiency of using the optimized median parameters for detecting the main coronary artery even though the existence of arteries of dissimilar shapes, sizes, and color in the presence of artifacts. From the above results and discussions, it is obvious that the median parameters values is the optimal set of values that perfect match the used dataset.

Figure 7 shows the detection outcomes related to the corresponding ground truth images. Fig. 7(c), (d), and (e) show the marked detected boundaries in blue, while the ground-truth boundary in red. These visual results specify that the proposed model provides highly harmonized detected vessels with the ground-truth results. Fig. 7(c) displays that the detected boundaries are highly harmonized with the ground-truth.

Figure 7 proved that the efficiency of the proposed model using the optimized median parameters for detecting the main coronary artery regardless of the existence of arteries having unlike sizes, shapes, and color. From the above results and discussions, it is obvious that the median parameters' values are the optimal set of values that provide perfect match to the used dataset.

Further, the optimization approach using the median parameters is compared with designed system by Kerkeni *et al.* [17] using the parameters stated in its approach. In [17], the used maximum radius value was σ_{max} which in our case is 13, 1 for σ_{min}, four log spacing between σ_{max} *and* σ_{min}, and 95% for α. Table 3 demonstrated that the tuned parameters are totally different from the proposed system by Kerkeni *et al.* [17], which means these parameters are based on the dataset under concern.

From the previous experiments, any change of these six parameters will have a direct effect on the segmented results, leading to different evaluation metrics' values. The evaluation metrics are also calculated for Kerkeni *et al.* [17] technique using default parameters as shown in Table 4.

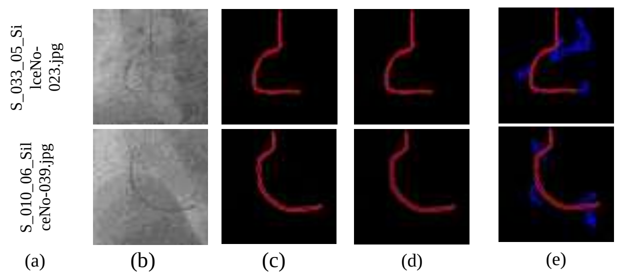

Figure 7. Proposed system detection results, where (a) image ID, (b) original image, (c) detection results using the median parameters, (d) detection results using the best parameters, and (e) detection results using the average parameters.

Table 3. The optimal values of configured parameters by the proposed model compared with their corresponding parameters by Kerkeni et al. [17].

Method	σ_{max}	σ_{min}	σ_{step}	α	N	d
Kerkeni *et al.* [17]	13	1	4	0.95	150	5
Proposed model	9.03	1.80	9.5	0.97	73	3

Table 4. Comparison in terms of the evaluation metrics between the proposed model and using Kerkeni et al. [17] on our dataset.

	JAC	DSC	SEN	SPEC	ACC
Proposed model	0.579	0.716	0.733	0.993	0.986
Kerkeni *et al.* [17]	0.397	0.558	0.962	0.958	0.958

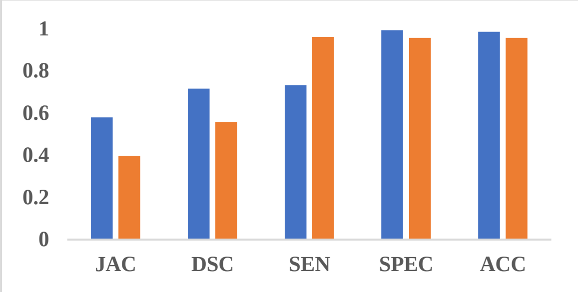

Figure 8. Comparison between the proposed model and the method by Kerkeni et al. [17] using our dataset in terms of the performance evaluation metrics, where the 'blue' bars indicate the proposed model results, and the 'orange' bars indicate the results of the method in [17].

Figure 8 validated that the proposed optimization method is accurately detects the main artery for the various cases. The dominance of the proposed method is due to the use of the optimized parameters in the Frangi filter, and the regional growing method that reduced the indeterminacy. It is also illustrated the dominance of the proposed optimized system compared to using the default parameters by decreasing the indeterminate information more powerfully because of using optimized Frangi with regional growing. Typically, the sensitivity and specificity represent the presence 'positive' or absence 'negative' the disease.

The sensitivity (true positive rate) refers to the probability of truly being positive, i.e. the probability of a branch being main coronary artery and it is actually main artery, while the specificity (true negative rate) refers to the probability of the detected branch to be truly being not a coronary artery. For all assessments and evaluations of the screening, and diagnostic, there is a trade-off between specificity and sensitivity, such that higher sensitivity means lower specificity and vice-versa. Since the main aim of the proposed model is detecting the coronary artery by searching only for main branch, the achieved accuracy and specificity values are superior to their corresponding ones using the model in [17]. Conversely, the model in [17] realized superior sensitivity compared to our proposed model, as reported in Table 4 and Fig. 8, as it concerned with detecting any minor branches as well. Typically, the proposed model searches only for the main branch, which is also proven with superior accuracy and specificity values compared to using the model in [17]. The comparative consequences of the evaluation metrics are illustrated in Fig. 9 using the proposed optimized parameters.

Figure 9 illustrates the dominance of the proposed model in comparison with using default parameters. Table 4 shows the mean of different performance metrics over the whole dataset. The results verified the preeminence of the proposed system for detecting the main artery with 71.6% average Dice compared to the results of the other methods.

4. Conclusion

Coronary artery computerized detection/segmentation is an inspiring process due to the intra-class discrepancy of low contrast and the artifacts in the X-ray angiography images. Numerous studies have been carried out to resolve these trials. In this paper, a novel main artery segmentation system was realized based on optimizing the value of Frangi with regional growing method in the X-ray angiography images.

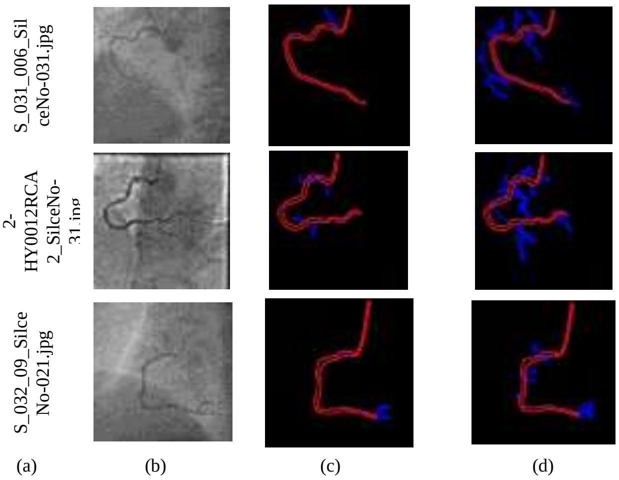

Figure 9. The proposed system detection results, where: (a) image ID, (b) original image, (c) detection results using Median parameters, and (d) detection results using default parameters by Kerkeni et al. [17].

The results of the proposed system proved that the optimal values of three Sigma parameters $\sigma_{\min}, \sigma_{\max}, \sigma_{step}$ are selected. These parameters control the vesselness response based on artery size according to the sigma that realized the highest JAC values (fitness function) throughout the GA optimization process. Five evaluation metrics were considered to compare the performance of the proposed system with other methods. The results proven the superiority of the proposed system with 71.6% average Dice over the results of other methods at different size, shape and uniformity of the main artery.

Funding: This research has not received any type of funding.

Conflicts of Interest: The author declares that there is no conflict of interest.

REFERENCES

[1] Frangi, A.F., W.J. Niessen, K.L. Vincken, and M.A. Viergever. *Multiscale vessel enhancement filtering*. in *International conference on medical image computing and computer-assisted intervention*. 1998. Springer.

[2] Jerman, T., F. Pernuš, B. Likar, and Ž. Špiclin. *Beyond Frangi: an improved multiscale vesselness filter*. in *Medical Imaging 2015: Image Processing*. 2015. SPIE.

[3] Jiang, X. and D. Mojon, *Adaptive local thresholding by verification-based multithreshold probing with application to vessel detection in retinal images.* IEEE Transactions on Pattern Analysis and Machine Intelligence, 2003. 25(1): p. 131-137.

[4] Cui, H. and Y. Xia, *Automatic coronary centerline extraction using gradient vector flow field and fast marching method from CT images.* IEEE Access, 2018. 6: p. 41816-41826.

[5] Teßmann, M., F. Vega-Higuera, B. Bischoff, J. Hausleiter, and G. Greiner, *Automatic detection and quantification of coronary calcium on 3D CT angiography data.* Computer Science-Research and Development, 2011. 26(1): p. 117-124.

[6] Cervantes, J., D. Luna, J. Cervantes, and F. García-Lamont. *Optimization of Vessel Segmentation Using Genetic Algorithms*. in *International Conference on Intelligent Computing*. 2022. Springer.

[7] Cruz-Aceves, I., F. Oloumi, R.M. Rangayyan, J.G. Aviña-Cervantes, and A. Hernandez-Aguirre, *Automatic segmentation of coronary arteries using Gabor filters and thresholding based on multiobjective optimization.* Biomedical Signal Processing and Control, 2016. 25: p. 76-85.

[8] Tenekeci, M.E., H. Pehlivan, and Y. Kaya, *Improving performance of coronary artery segmentation using calculated vessel location from the angiogram.* Biomedical Research, 2018. 29(1): p. 130-136.

[9] Jin, J., L. Yang, X. Zhang, and M. Ding, *Vascular tree segmentation in medical images using Hessian-based multiscale filtering and level set method.* Computational and mathematical methods in medicine, 2013. 2013.

[10] Demirel, H., G. Anbarjafari, and M.N.S. Jahromi. *Image equalization based on singular value decomposition*. in *2008 23rd International Symposium on Computer and Information Sciences*. 2008. IEEE.

[11] Khawaja, A., T.M. Khan, K. Naveed, S.S. Naqvi, N.U. Rehman, and S. Junaid Nawaz, *An Improved Retinal Vessel Segmentation Framework Using Frangi Filter Coupled With the Probabilistic Patch Based Denoiser.* IEEE Access, 2019. 7: p. 164344-164361.

[12] Zuiderveld, K., *Contrast limited adaptive histogram equalization.* Graphics gems, 1994: p. 474-485.

[13] He, K., J. Sun, and X. Tang, *Guided image filtering.* IEEE transactions on pattern analysis and machine intelligence, 2012. 35(6): p. 1397-1409.

[14] Langford, E., *Quartiles in elementary statistics.* Journal of Statistics Education, 2006. 14(3).

[15] Lindeberg, T., *Principles for automatic scale selection.* 1999.

[16] Lorenz, C., I.-C. Carlsen, T.M. Buzug, C. Fassnacht, and J. Weese. *Multi-scale line segmentation with automatic estimation of width, contrast and tangential direction in 2D and 3D medical images*. in *CVRMed-MRCAS'97*. 1997. Springer.

[17] Kerkeni, A., A. Benabdallah, A. Manzanera, and M.H. Bedoui, *A coronary artery segmentation method based on multiscale analysis and region growing.* Computerized Medical Imaging and Graphics, 2016. 48: p. 49-61.

[18] Ashour, A.S., A.R. Hawas, Y. Guo, and M.A. Wahba, *A novel optimized neutrosophic k-means using genetic algorithm for skin lesion detection in dermoscopy images.* Signal, Image and Video Processing, 2018. 12(7): p. 1311-1318.

[19] Hawas, A.R., Y. Guo, C. Du, K. Polat, and A.S. Ashour, *OCE-NGC: A neutrosophic graph cut algorithm using optimized clustering estimation algorithm for dermoscopic skin lesion segmentation.* Applied Soft Computing, 2020. 86: p. 105931.

[20] Ashour, A.S., C. Du, Y. Guo, A.R. Hawas, Y. Lai, and F. Smarandache, *A novel neutrosophic subsets definition for dermoscopic image segmentation.* IEEE Access, 2019. 7: p. 151047-151053.